Impact of the South and North Pacific Meridional Modes on the El Niño–Southern Oscillation: Observational Analysis and Comparison

QINGYE MIN

State Key Laboratory of Severe Weather, Chinese Academy of Meteorological Sciences, Beijing, and Institute of Atmospheric Sciences, Fudan University, Shanghai, China

JINGZHI SU

State Key Laboratory of Severe Weather, Chinese Academy of Meteorological Sciences, Beijing, China

RENHE ZHANG

State Key Laboratory of Severe Weather, Chinese Academy of Meteorological Sciences, Beijing, and Institute of Atmospheric Sciences, Fudan University, Shanghai, China

(Manuscript received 11 January 2016, in final form 27 October 2016)

ABSTRACT

An interannual variability mode in the southeast Pacific with a physical interpretation similar to that of the Pacific meridional mode (PMM) in the North Pacific was recently identified. Both modes have been shown to influence the subsequent development of El Niño–Southern Oscillation (ENSO) events. This study investigates the relationship between ENSO and the two PMMs using observational and reanalysis data. The results show that the South Pacific meridional mode (SPMM) mainly favors the development of sea surface temperature anomalies (SSTAs) in the eastern equatorial Pacific, whereas the North Pacific meridional mode (NPMM) mainly favors the development of SSTAs in the central equatorial Pacific. Both of the meridional modes are considered to be analogous in terms of their physical interpretation and can be important predictors of ENSO when considering different flavors of ENSO. Neither the NPMM nor the SPMM can be precluded as accurate indicators when forecasting particular flavors of ENSO.

1. Introduction

As the most prominent source of interannual climate variability, the El Niño–Southern Oscillation (ENSO) phenomenon has significant impacts on global climate patterns. In recent decades, our ability to predict ENSO events has gradually improved because of improved understanding of the tropical oceanic–atmospheric processes underlying the ENSO phenomenon and continuous improvements in observation, analysis, and assimilation systems (e.g., McPhaden et al. 1998; Guilyardi et al. 2009; Barnston et al. 2012). Over the past two decades, numerous studies have established a robust relationship between the development of ENSO and the extratropical variability of the atmosphere (e.g., Pierce et al. 2000; Vimont et al. 2003a,b), and the linkage is maintained via internal atmospheric and oceanic dynamics (e.g., Servain et al. 1999; Kushnir et al. 2002). Vimont et al. (2001) were among the first to suggest that a physical connection occurred between extratropical atmospheric variability over the North Pacific during a specific boreal winter and ENSO in the following year, and they proposed the seasonal footprinting mechanism (SFM) to explain the physical connection. In the North Pacific, the North Pacific Oscillation (NPO) (Rogers 1981) manifests as large-scale sea level pressure oscillations. The variability of the semipermanent subtropical high pressure system caused by the NPO effectively modulates the strength of the northeasterly trade winds in the tropical latitudes and leaves an anomalous footprint on sea surface temperatures (SSTs) via changes in wind-induced latent heat

---

∂ Denotes content that is immediately available upon publication as open access.

Corresponding author e-mail: Dr. Su Jingzhi, sujz@camscma.cn

fluxes in the boreal winter and spring. The relevant meridional SST gradient can persist into the boreal summer and then induce atmospheric circulation changes in the tropical Pacific (Vimont et al. 2001). Chiang and Vimont (2004) suggested that such a meridional SST gradient can displace the intertropical convergence zone (ITCZ). Moreover, changes in the winds that modify local heat fluxes can feed back into the SST gradient and generate a covarying pattern between the ITCZ and the north–south SST gradient in the tropical North Pacific. This covarying pattern has been referred to as the North Pacific meridional mode (NPMM) of variability (Chiang and Vimont 2004) because of the similarities in climatology between the Pacific and Atlantic as well as the well-established Atlantic meridional mode (Nobre and Shukla 1996; Chang et al. 1997).

Recent studies have shown that most El Niño events in recent decades have been preceded by apparent NPMM (positive phase) activity. For example, Chang et al. (2007) argued that the NPMM effectively acts as a conduit through which the extratropical atmosphere influences ENSO. Yu et al. (2010) reaffirmed that subtropical forcing is necessary for interannual SST variability in the equatorial Pacific and argued that the subtropical Pacific, particularly the subtropical North Pacific, may play an important role in the initiation of the central Pacific El Niño. Vimont et al. (2009) also performed numerical experiments demonstrating that the seasonality of NPO-related atmospheric variability and subtropical air–sea thermodynamic coupling in the North Pacific plays a fundamental role in the seasonal phase-locking behavior of ENSO. Recently, Di Lorenzo et al. (2015) further confirmed that the El Niño–like interdecadal pattern could also be established through the combined actions of the Pacific meridional modes and ENSO.

Numerous studies have been devoted to the significant influence of the North Pacific variability on the evolution of ENSO; however, comparatively few investigations have examined the influences of the South Pacific on ENSO. Studies by Zhang et al. (2001) and Zhang and Zhao (2001) showed that significant meridional wind stress anomalies appear over the eastern tropical South Pacific more than half a year prior to ENSO. The convergence of the southerly wind stress anomalies around the equator with the northerly wind stress anomalies over the tropical eastern North Pacific is an important factor in initiating an El Niño event. Zhang et al. (2014a,b) investigated the connection between the South Pacific atmospheric variability and tropical Pacific climate using both observational data and models, and their results showed that the Pacific meridional mode in the Southern Hemisphere, defined as the South Pacific meridional mode (SPMM), has a larger equatorial signature than the NPMM for the same amount of extratropical variability, particularly in the eastern equatorial Pacific. The authors also argued that the physical interpretation of the SPMM is nearly identical to that of the NPMM, with the variability in the off-equatorial southeast trade winds altering the latent heat flux and SSTs and initiating a wind–evaporation–SST (WES) feedback (Xie and Philander 1994) that propagates signals into the tropics.

In general, the predictability of ENSO events, particularly the specific flavors of ENSO, are closely related to atmospheric and/or oceanic precursors responsible for the excitation of events at certain lead times (U.S. CLIVAR ENSO Diversity Working Group 2013). El Niño events can be classified based on particular spatial patterns of SST anomalies (SSTAs) as either the eastern Pacific (EP) type or the central Pacific (CP) type (e.g., Ashok et al. 2007; Kao and Yu 2009; Kug et al. 2009; Chen et al. 2015). Hence, it is important to further investigate the relative roles of the NPMM and the SPMM in generating ENSO. Specific questions of interest include the following: What are the differences between the NPMM and the SPMM in terms of seasonal characteristics? What are the specific differences between the influence of the NPMM and the SPMM on ENSO? Is the SPMM of significance for ENSO predictions based on the different flavors of ENSO? To answer these specific questions, the relationship between the intrinsic atmospheric variability and the meridional modes that may act as the effective stochastic forcing of ENSO must be examined and described in more detail using a reanalysis of atmospheric data. The data and methodology are introduced in section 2. By removing the linear influence of ENSO from the reanalysis data, the dominant modes of the atmosphere–ocean variability extracted from the tropical North and South Pacific are investigated in terms of spatial and temporal characteristics in section 3. Because the NPMM has been well investigated in previous studies, the structure of the SPMM in the South Pacific and its influence on ENSO are presented in more detail relative to its Northern Hemisphere counterpart in section 4. In section 5, the physical interpretation of the SPMM is further investigated and a comparison between the physical interpretations of the NPMM and SPMM is presented. A summary and discussion of our results are provided in section 6.

2. Data and methodology

The monthly mean SST and 10-m wind data used in this study are from the National Centers for Environmental Prediction–National Center for Atmospheric Research (NCEP–NCAR) Reanalysis 1 project (Kalnay et al. 1996), which spanned the period of January 1948–December
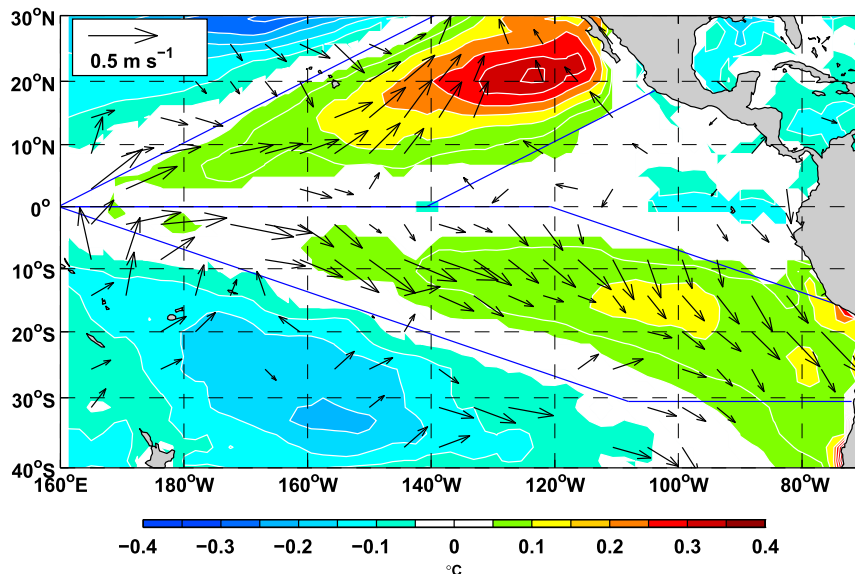
FIG. 1. Regression maps of the MCA leading mode SST-normalized expansion coefficients for the SST and 10-m wind vectors. Shaded regions are significant at the 95% confidence level, and only surface wind vectors significant at the 95% confidence level are plotted. The blue lines indicate the parallelogram areas used in the MCA analysis for the North Pacific and South Pacific.

2014. Here, detrended monthly mean anomalies were calculated, and a 3-month running mean was applied for each field.

The maximum covariance analysis [MCA, also known as singular value decomposition; Bretherton et al. (1992)] was applied to the cross-covariance matrix between the SST and both components of the 10-m winds. The influence of the NPMM and SPMM on ENSO is difficult to detect directly from the original data because the relatively weak characteristics of the two modes are overwhelmed by the prominent ENSO signals. Therefore, a method that performs a linear squares fit to a commonly used cold tongue index [CTI; SSTAs averaged over 6°S–6°N and 180°–90°W (Deser and Wallace 1990)], which was previously used by Chiang and Vimont (2004), was applied. The linear least squares fit to the CTI was subtracted from all fields prior to the MCA analysis, and then both the NPMM and the SPMM variabilities that are linearly independent of ENSO were obtained, and the time-lag influences of the NPMM and the SPMM on ENSO were investigated. Because the NPMM–SPMM is expressed by the first mode of the corresponding MCA in the present analysis, only the leading modes are discussed in the following sections.

3. Two meridional modes

First, the MCA analyses for both meridional modes were performed in the vicinity of the tropical Pacific basin (40°S–30°N, 160°E–90°W). Both regression maps of the MCA leading mode SST normalized expansion

coefficient on the SST and 10-m wind vectors are shown in Fig. 1. The squared covariance fraction for the leading mode was 42%. Two dominant loadings were located in the subtropics in both the North Pacific and South Pacific, which represented the NPMM and SPMM, respectively. Because the main patterns of the NPMM–SPMM are not rectangular but inclined regions, we changed the rectangular areas [used by Chiang and Vimont (2004)] to parallelogram areas and applied the MCA analysis to both regions. To illustrate the different characteristics of each mode, the MCA analyses were independently performed on two parallelogram domains in the North and South Pacific (Fig. 1). The squared covariance fractions for both leading modes were greater than 70% (Figs. 2a,b), thus explaining the majority of the total squared covariance. The spatial structures of the leading MCA modes are shown in the regression maps of the SST and 10-m winds onto the normalized SST expansion coefficients for the North Pacific (Fig. 2a) and South Pacific (Fig. 2b). The SST regression map obtained in the North Pacific (Fig. 2a) was highly similar to that obtained in the tropical Pacific (Fig. 1) and presented a spatial correlation of 0.77 over 20°S–30°N and 160°E–90°W. Similarly, the spatial correlation between the SST regression map obtained for the South Pacific (Fig. 2b) and those obtained for the Pacific (Fig. 1) was 0.96 over the region of 40°S–10°N and 180°–70°W. The South Pacific pattern strongly resembled the North Pacific pattern that emerged with SSTAs in the subtropical Pacific region, thereby
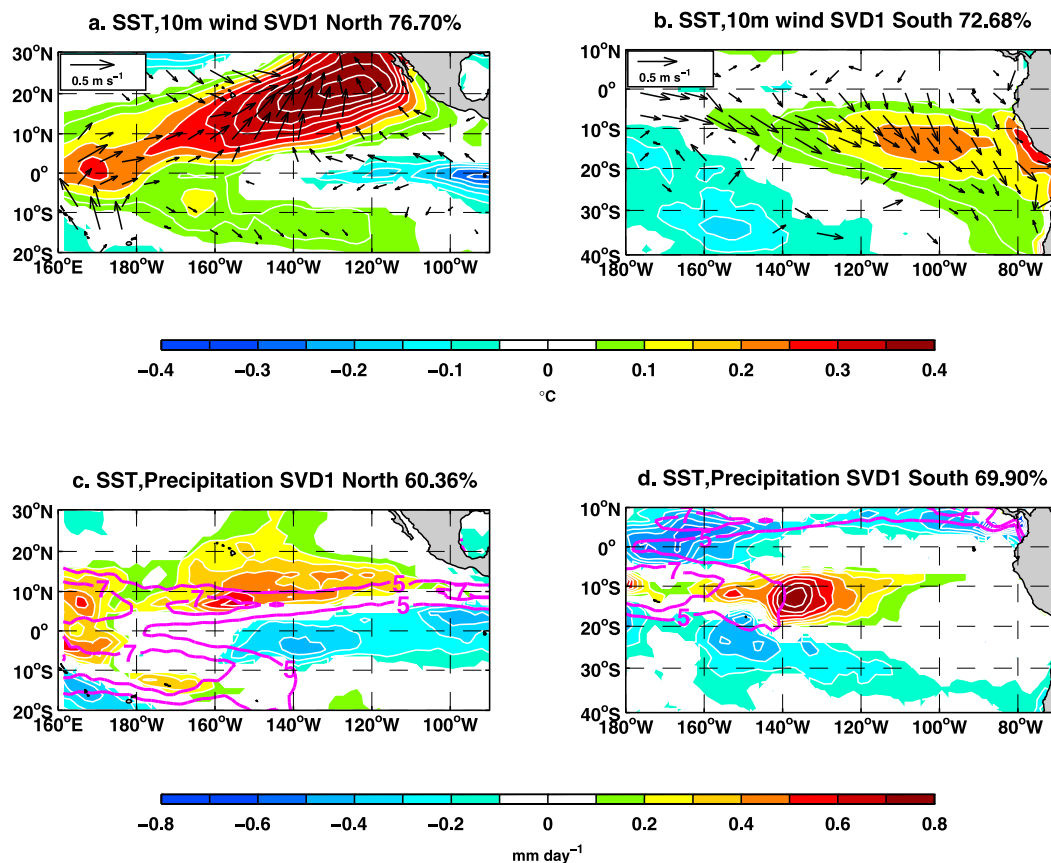
FIG. 2. Spatial properties of the MCA mode 1 in the (left) North Pacific and (right) South Pacific. (a),(b) Regression maps of the MCA leading mode SST-normalized expansion coefficients of the SST and 10-m wind vectors. (c),(d) As in (a),(b), but for precipitation. The climatological mean precipitations are indicated by magenta heavy contours. Shaded regions in all panels are significant at the 95% confidence level. Only surface wind vectors significant at the 95% confidence level are plotted.

producing an anomalous meridional SST gradient. Both leading MCA modes were identical to the corresponding second MCA modes derived directly from the original data (without removing the CTI via linear regression; not shown). The SST and 10-m wind patterns (Fig. 2b) were nearly identical to the SPMM introduced by Zhang et al. (2014a); therefore, we define this pattern as the SPMM in this study. The MCA modes were also performed between SSTs and precipitation (Figs. 2c,d). Similar to the NPMM (positive phase), which favored an anomalous northeastward displacement of the ITCZ in the central Pacific (Fig. 2c), the SPMM (positive phase) favored an anomalous eastward displacement of the ITCZ in the central Pacific (Fig. 2d). It is worth noting that if ENSO influences are removed in a manner similar to that performed by Chiang and Vimont (2004), then the obtained SPMM does not change (not shown).

A question remains as to whether the SPMM is merely a residual of the NPMM in the subtropical southeast Pacific. To address this issue, the temporal

characteristics of the leading modes were further investigated. Because the CTI was removed from all fields before the MCA, the correlation between the CTI and the NPMM (SPMM) SST expansion coefficients was nearly zero (Figs. 3e,g). The SST expansion coefficients in both the NPMM and SPMM had apparent interannual variabilities (1 ~ 2 yr) (Figs. 3f,h). However, the correlation between the SST expansion coefficients of the NPMM and SPMM was weak ($r = 0.24$), indicating that the two modes varied independently in the North and South Pacific. The year-to-year variance of the SST expansion coefficient (Fig. 3a) for the NPMM peaked in the boreal spring, and the wind variance peaked in the late boreal winter–early boreal spring. In contrast, the year-to-year variance of the SST expansion coefficient (Fig. 3b) for the SPMM peaked in the boreal winter, and the wind variance reached a weak peak in the late boreal winter/early boreal spring. Therefore, the seasonal characteristics of the SPMM differed from those of the NPMM. A lagging correlation between the
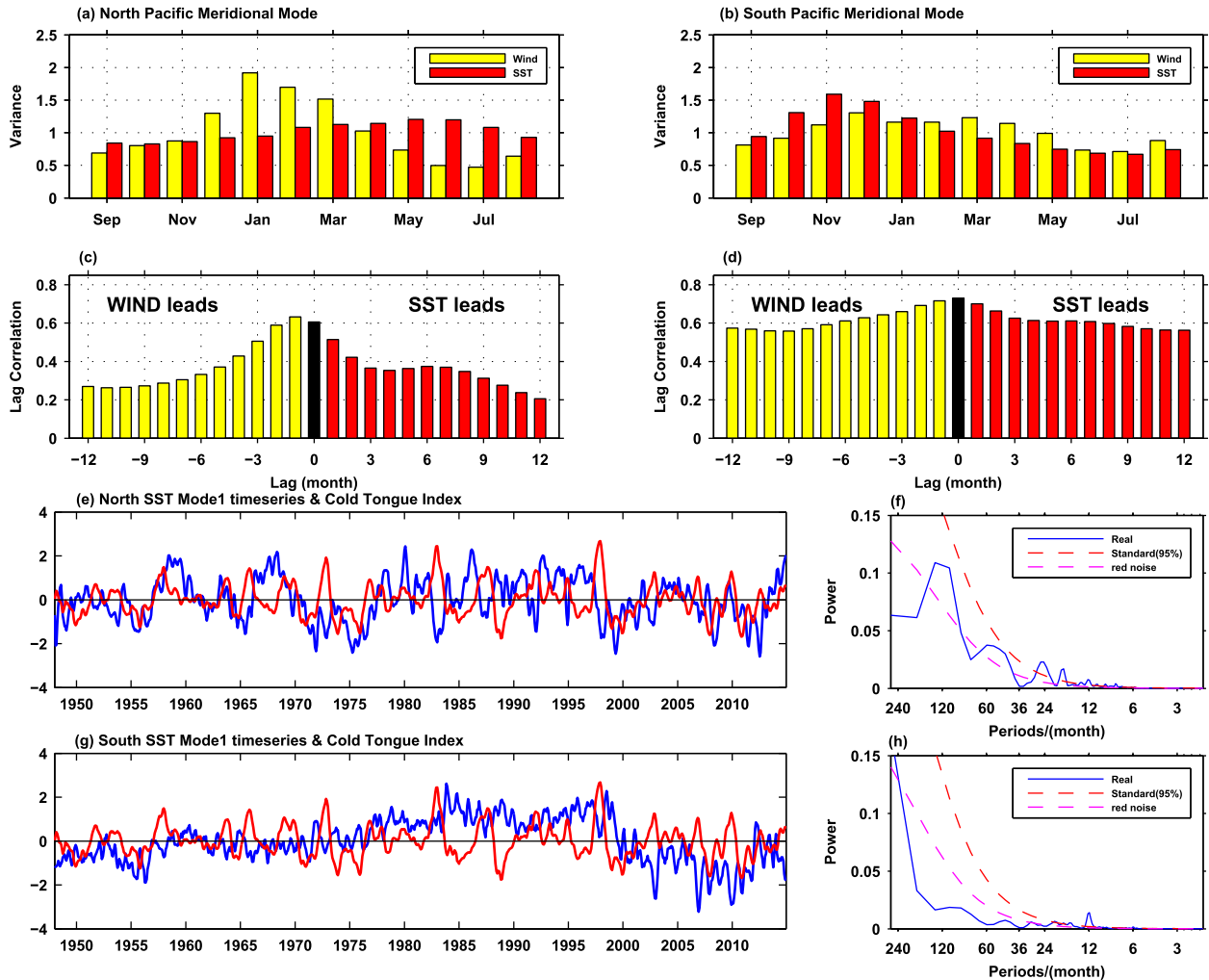
FIG. 3. Temporal properties of the leading MCA mode: Variance in the (a) North Pacific and (b) South Pacific calculated by the month for the SST (red shading) and for the wind (yellow shading) expansion coefficients. (c),(d) Lagged correlation between the SST and 10-m wind expansion coefficients for North and South Pacific, respectively. The black bar shows simultaneous correlations and yellow (red) shaded bars are for winds leading (lagging) SST. For reference, correlations > 0.24 are significant at the 95% confidence level assuming a decorrelation time scale of 1 yr (67 independent samples). (e),(g) SST expansion coefficients for the North Pacific and South Pacific MCA mode 1 (blue curve) and cold tongue index (red curve), respectively. (f),(h) Power spectra of the SST expansion coefficients for the North Pacific and South Pacific MCA mode 1, respectively. The dashed magenta line denotes red noise and the dashed red line denotes the 95% significance curve.

NPMM expansion coefficients showed that the wind variation preceded the SST variation by one month (Fig. 3c), and the contemporaneous correlation between the SPMM expansion coefficients was the largest (Fig. 3d), which means that winds and SST mutually drive each other.

4. Relationship between ENSO and North–South Pacific meridional modes

Does the linear removal of the CTI from the original fields sufficiently remove the ENSO effect so that the surface wind pattern coupled with the SST pattern is independent of ENSO? Neither ENSO in the previous boreal winter (relative to the PMMs) nor the concurrent ENSO produces apparent effects on the two surface wind patterns (Figs. 4a–d). Figures 4a,b show scatterplots of an interannual ENSO index against the seasonal normalized values of the NPMM–SPMM 10-m wind expansion coefficient. The ENSO index is defined as the CTI averaged over November–December–January [NDJ(−1), which means ND(−1) and J(0), 0 indicates the current year, −1 indicates the previous year, and +1 indicates the following year]. The seasonal values of 10-m wind expansion coefficient is averaged over
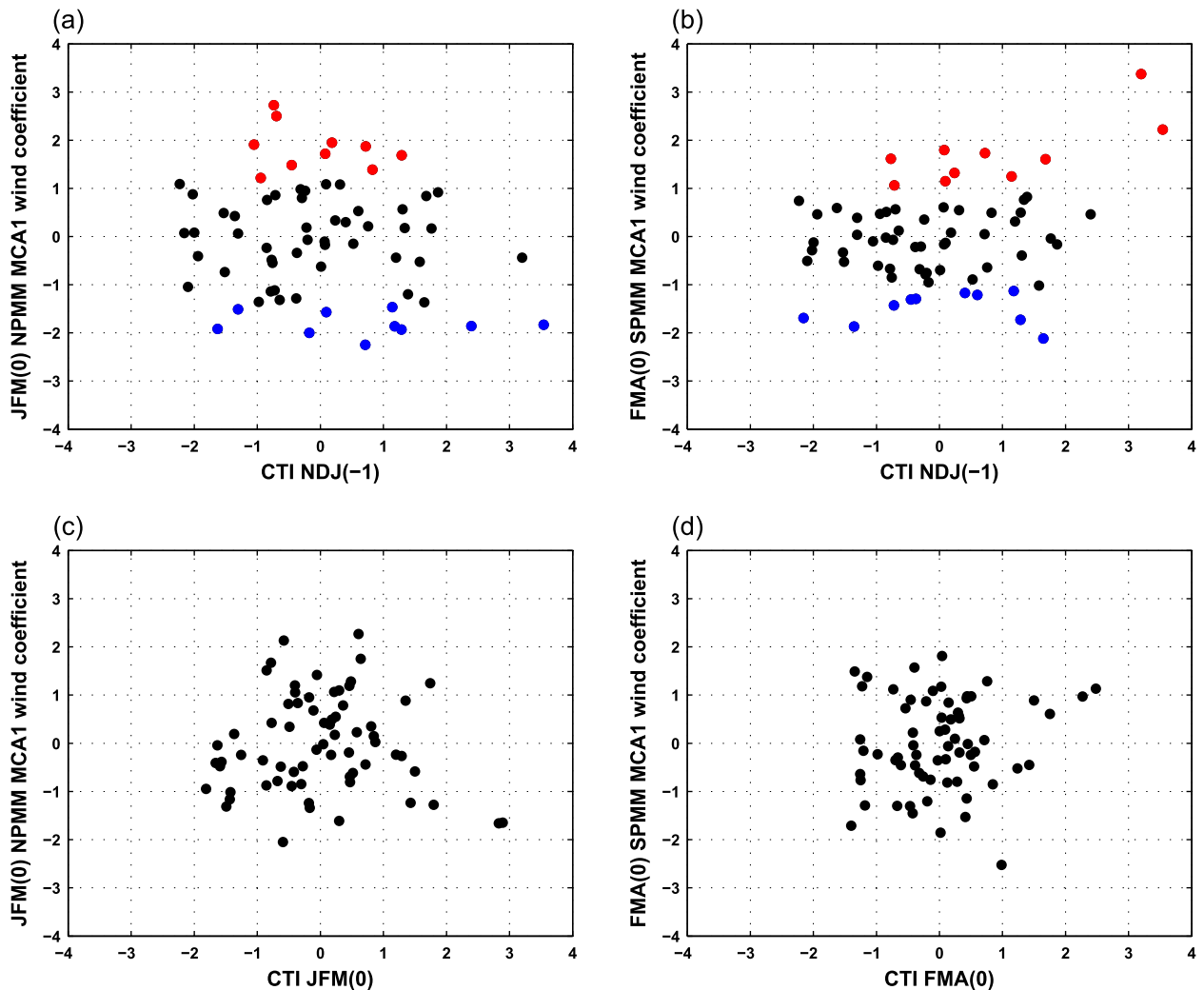
FIG. 4. (a) JFM(0)-averaged values of the North Pacific MCA 1 10-m wind expansion coefficients vs NDJ(−1)-averaged CTI. (b) As in (a), but for FMA(0)-averaged values of the South Pacific MCA. (c) As in (a), but vs JFM(0)-averaged CTI. (d) As in (c), but vs FMA(0)-averaged CTI. The red (blue) points indicate the selected years [positive (negative)] in the composite analysis.

January–February–March [JFM(0)] for the NPMM, but it is averaged over February–March–April [FMA(0)] for the SPMM. We choose JFM–FMA here because the corresponding behavior of the 10-m winds in this period was most pronounced for the NPMM–SPMM (Figs. 3a,b). Visual examination of the scatterplot did not suggest that extreme ENSO events tend to favor a particular trend in the NPMM 10-m wind expansion coefficient (Fig. 4a), and this finding was also observed for the SPMM (Fig. 4b). The relationship between the NPMM–SPMM surface wind patterns and the concurrent ENSO (Figs. 4c,d) is similar to that associated with ENSO in the previous boreal winter (relative to PMMs) (Figs. 4a,b). These results indicate that ENSO does not project a significant influence on the surface wind patterns of the NPMM and SPMM. It is worth noting that the SST

expansion coefficient for both the NPMM and SPMM exhibits a type of nonlinear behavior with the CTI as was shown in Chiang and Vimont (2004) (not shown). However, the following analysis is based on the 10-m wind expansion coefficient, and the nonlinear behavior of PMM SST patterns are beyond the scope of this study.

Because the surface wind variabilities of both the NPMM and SPMM in the previous boreal winter were independent of ENSO, we defined two annual indexes associated with the MCA modes by averaging the JFM MCA 10-m wind expansion coefficient of the NPMM and the FMA MCA 10-m wind expansion coefficient of the SPMM. Then, the regressed patterns for the anomalies of surface level pressure (SLP), zonal wind stress, SST, and surface latent heat flux (Figs. 5 and 6) were
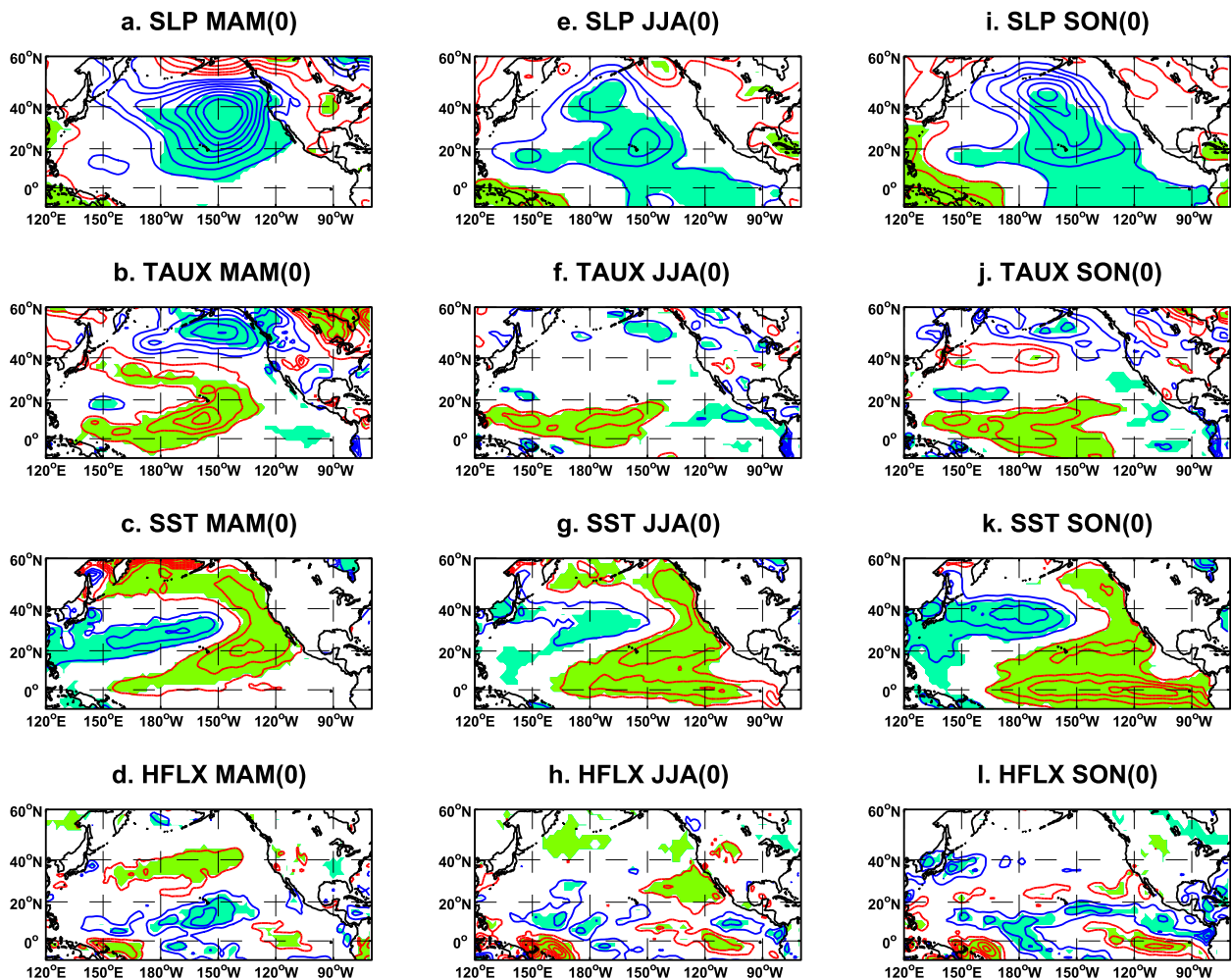
FIG. 5. Regression maps of the (left) boreal spring (MAM averaged), (middle) summer (JJA averaged), and (right) autumn (SON averaged): (top to bottom) SLP (mb; contours with 0.1 mb interval), zonal wind stress (N m^{-2}; contours with 2.5×10^{-3} N m^{-2} interval), SST (°C; contours with 0.1°C interval), and surface latent heat flux (W m^{-2}; contours with 2 W m^{-2} interval) anomalies on the JFM(0)-averaged 10-m wind expansion coefficients of North Pacific MCA mode 1. The shaded regions in all panels are significant at the 95% confidence level.

obtained from a lagged regression against the above annual indexes of the NPMM and SPMM. Because the principal aim of this section is to investigate the impacts of NPMM–SPMM on ENSO, the regression and composite analyses were performed based on the original data to obtain seasonal variations associated with ENSO, and the CTI was not linearly removed.

The processes associated with the NPMM (Fig. 5) have been investigated and interpreted in previous studies (e.g., Vimont et al. 2001, 2003a,b). In the subtropical North Pacific, decreased northern subtropical trade winds are accompanied by a decrease in latent heat flux out of the ocean, an increase in the westerly wind stress, and an increase in the SST of the northeastern Pacific (Fig. 5). Such phenomena could persist into the boreal summer with a positive latent heat flux

anomaly (positive downward) and westerly wind stress propagating to the equator, thereby causing a southwesterly extension of SSTAs and ultimately affecting the development of equatorial SSTAs in the boreal summer–autumn.

In the south subtropical Pacific, decreases in the southern subtropical trade winds during late boreal winter and early boreal spring (FMA) coincide with a decrease in the latent heat flux from the ocean, an increase in the westerly wind stress and an increase in the SST, particularly near the coastline of South America (Fig. 6). Such phenomena could persist into the boreal summer and autumn with a positive latent heat flux anomaly (positive downward) and westerly wind stress propagating to the equator, which is associated with a northwesterly extension of SSTAs. The location of the
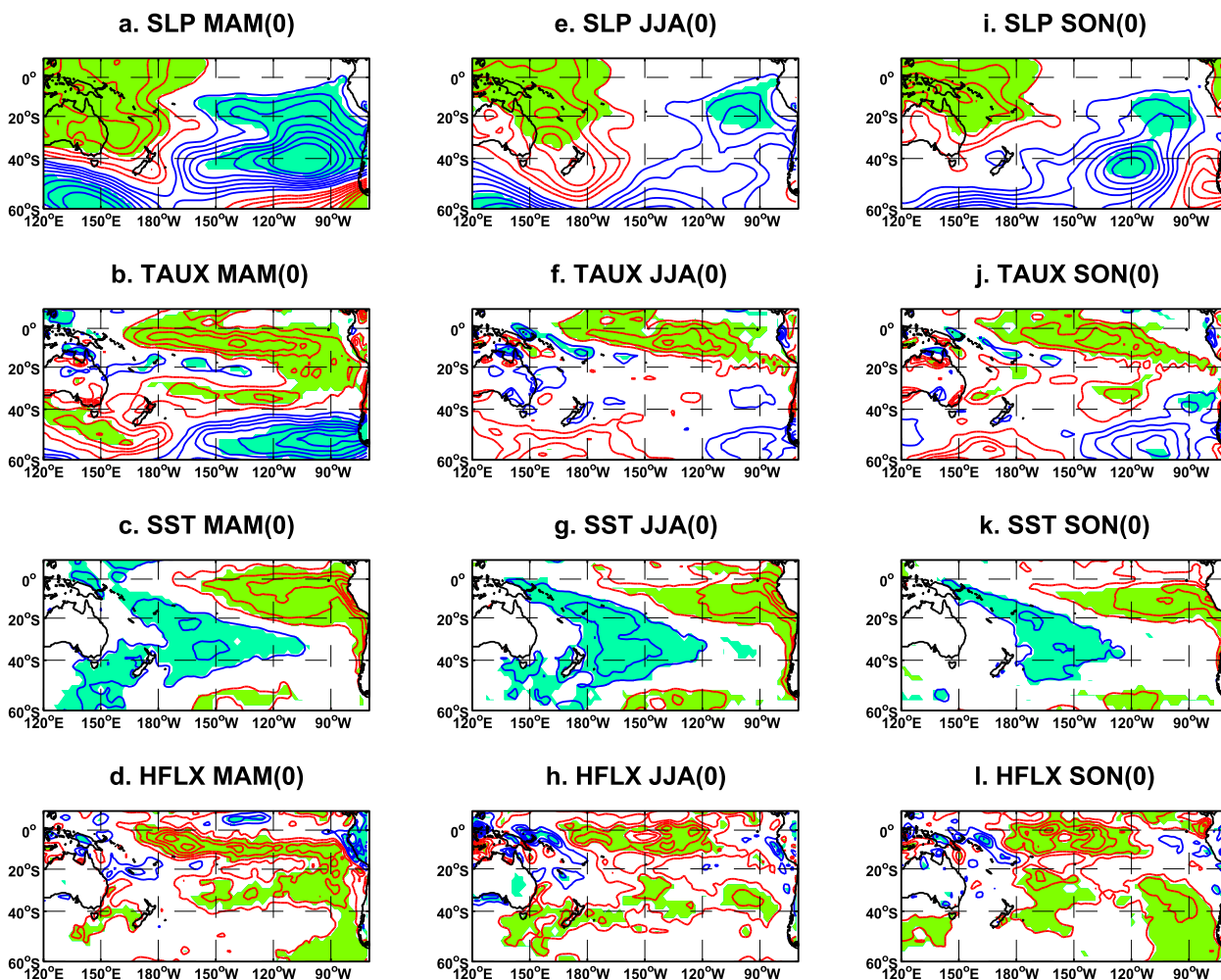
FIG. 6. As in Fig. 5, but for anomalies on the FMA(0)-averaged 10-m wind expansion coefficients of South Pacific MCA mode 1.

SPMM (approximately 160°–70°W) is more eastward compared to that of the NPMM (approximately 160°E–120°W). Hence, the SPMM more easily influences the eastern equatorial Pacific SSTAs than the central equatorial Pacific SSTAs, whereas the influence of the NPMM exhibits the opposite trend. Zhang et al. (2014b) further proposed that the interhemispheric asymmetry between the PMMs is largely attributed to the asymmetric mean trades in the Pacific. For both the NPMM and SPMM, the anomalous westerlies in the western equatorial Pacific may excite downwelling equatorial Kelvin waves, which in turn deepen the thermocline in both the central and eastern Pacific and increase the amplitude of SSTAs (Figs. 5b,c,f,g,j,k and Figs. 6b,c,f,g,j,k).

To confirm that the regressed results presented above were robust, composite analyses were conducted. The composite NCEP reanalysis monthly mean SST and 10-m wind fields were calculated based on the high and low years of the JFM-averaged 10-m wind expansion

coefficients of the NPMM (Fig. 4a). Similarly, such composite fields were calculated for the SPMM based on its FMA-averaged 10-m wind expansion coefficients (Fig. 4b). The composites of the NPMM- (SPMM-) affected years were from the 10 largest positive and negative values of the JFM- (FMA-)averaged 10-m wind expansion coefficients (obtained for all 66 yr). The chosen years are shown in Table 1 and Fig. 4 (red and blue points). For both meridional modes, the means of the high- and low-value years for each 3-month interval from the boreal spring (March–May) through the autumn (September–November) were calculated first, and then their difference was calculated and divided by 2 (Fig. 7). It is worth noting that the selected years do not overlap to avoid mixing signals from the two PMMs (Table 1).

The composites (Figs. 7a–c for the NPMM, Figs. 7d–f for the SPMM) show the evolution of the NPMM and SPMM for the SST and 10-m wind anomalies. The

TABLE 1. NPMM- and SPMM-affected years used in the composites analysis. For the NPMM, those years were taken around the 10 largest positive and negative values of the JFM averaged 10-m wind expansion coefficient for all 66 yr. For the SPMM, years were taken in the vicinity of the 10 largest positive and negative values of the FMA-averaged 10-m wind expansion coefficient for all 66 yr. Years selected in the composite analysis are set bold.

NPMM	+	1963 **1965 1968 1978** 1980 **1982 1986** 1993 **1995 1996**
	−	**1952 1953** 1964 **1973** 1977 1998 **1999** 2007 **2012 2013**
SPMM	+	1977 1980 **1981 1983 1984 1992** 1993 **1994 1997** 1998
	−	**1954 1955 1956 1959** 1963 1964 **2002** 2007 **2010 2011**

results of the regression analysis were confirmed by the composite analyses. First, the SSTAs in the northern subtropical region reached their maximum in the boreal spring and were accompanied by SST-driven meridional circulation that coincided with the maximum meridional SST gradient. Second, the northern subtropical SSTAs began to decay starting in the boreal summer, and then the central equatorial SSTAs began to develop. In contrast, the SSTAs in the subtropical southern region were maintained from the boreal spring and accompanied by a corresponding meridional SST gradient. The SST-driven meridional circulation in the subtropical southeastern Pacific was relatively significant from the boreal spring to the autumn. Moreover, the offshore SSTAs along South America were maintained with a strong signal from boreal spring to autumn.

5. Interpretation of the SPMM and implications for ENSO

Vimont et al. (2003b) confirmed a robust relationship between the November–March(−1) [ND of year(−1) and JFM of year(0)] North Pacific extratropical SLP, the April–August(0) North Pacific tropical surface zonal wind stress (UFLX), and the October–February(0) [OND of year(0) and JF of year(+1)] tropical Pacific SSTs [Figs. 8a and 9, which are similar to Figs. 2 and 3 of Vimont et al. (2003b)]. These authors further suggested that such a strong relationship may enhance the predictability of ENSO. The conclusions in section 4 reinforce the possibility of introducing a subtropical precursor to enhance ENSO predictions. Additionally, the subtropical precursor in the Southern Hemisphere, which presents different behaviors and influences than the NPMM in our interpretation, was as important as the subtropical precursor in the Northern Hemisphere when considering its contribution to a different flavor of ENSO. Thus, performing moderately accurate predictions of the SSTA patterns before the initiation of ENSO may be possible by considering the two leading MCA modes. Because the North Pacific pattern and its

implications for ENSO have been well studied and analyzed (e.g., Vimont et al. 2003b; Chiang and Vimont 2004), this section focuses on the South Pacific pattern and its implications for ENSO. To further investigate the lagging coupled relationship between the SPMM and ENSO, a MCA with the three pairs of variables for the period 1948–2014 was performed following Vimont et al. (2003b): January–May(0) South Pacific extratropical SLP, June–October(0) South Pacific tropical surface zonal wind stress (UFLX), and November–March(0) [ND of year(0) and JFM of year(+1)] tropical Pacific SST. The terms January–May(0), June–October(0), and November–March(0) refer to the consecutive seasons over which the extratropical SLP (JFMAM), tropical surface zonal wind (JJASO), and tropical SST (NDJFM) were averaged in the analysis, respectively.

The spatial and temporal domains of the data used to generate the leading modes of the MCA-I [JFMAM(0) South Pacific extratropical SLP and JJASO(0) South Pacific tropical surface zonal wind], MCA-II [JFMAM(0) South Pacific extratropical SLP and NDJFM(0) tropical Pacific SST], and MCA-III [JJASO(0) South Pacific tropical surface zonal wind and NDJFM(0) tropical Pacific SST] are shown in Fig. 8b. As suggested by Vimont et al. (2003b), the ONDJF(−1) responses to the CTI were removed from the data before analysis to ensure that both the JJASO(0) tropical zonal wind and the NDJFM(0) tropical SST were independent of any ENSO variability that may have occurred during the preceding winter. The statistical results from the MCA are summarized in Fig. 8b, which indicates that the fields included in the analysis were as strongly coupled as their counterparts in the Northern Hemisphere (Fig. 8a). The leading pairs of heterogeneous regression maps resulting from the MCA are presented in Figs. 9 and 10. The correlation is shaded, and it is only displayed where it is statistically significant at a 95% confidence level.

Figures 10a and 10b show the leading pair of coupled patterns for the MCA-I [JFMAM(0) Southern Hemisphere midlatitude SLP and JJASO(0) Southern Hemisphere tropical zonal wind stress]. The South Pacific extratropical SLP pattern in Fig. 10a shows a triple SLP pattern with two centers on the north side at approximately 30°S and one center on the south side. This pattern may play a similar role as the NPO in the Northern Hemisphere, particularly in the northern lobe of this pattern (around 40°–15°S, 180°–90°W), which is indicative of weakened trades throughout the subtropics. The reduced trades are important for forcing the subtropical portion of the SST footprint via a reduction of the upward latent heat flux (Fig. 6). During the
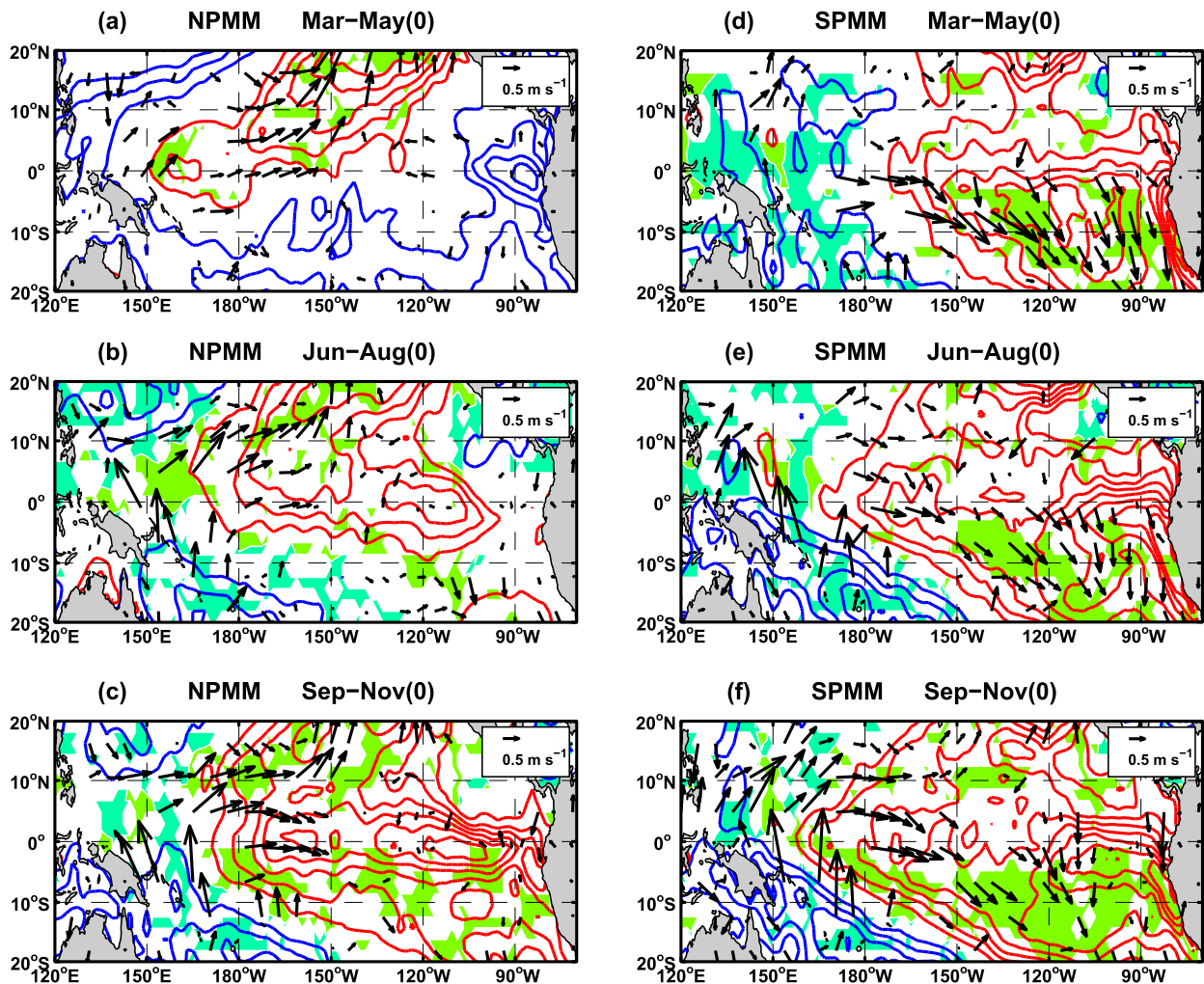
FIG. 7. (a)–(c) Composite analysis of the Pacific meridional mode based on positive and negative values of the JFM(0) 10-m wind expansion coefficients of North Pacific MCA mode 1. (d)–(f) As in (a)–(c), but based on the FMA(0) 10-m wind expansion coefficients of South Pacific MCA mode 1. The composites are in 3-month averages (top to bottom) from MAM(0) through the following SON(0). The maps were generated by subtracting the mean of the "negative" years from the mean of the "positive" years and then dividing by 2. Shown are the SST (contours with a 0.1°C interval) and 10-m wind (reference vector of 0.5 m s^{-1}) differences. The regions where the SST is statistically significant at the 0.05 level are shaded. Wind contours are plotted where the wind is statistically significant at the 95% confidence level.

following boreal summer, the tropical zonal wind (Fig. 10b) was dominated by positive anomalies in the central tropical Pacific, particularly in the Southern Hemisphere, and extending to the equator. The response of the subtropical zonal wind in the Southern Hemisphere was as strong as its counterpart in the Northern Hemisphere (Fig. 9b).

The results from the MCA-II [JFMAM(0) South Pacific extratropical SLP and NDJFM(0) tropical Pacific SST] are plotted in Figs. 10c and 10d. The SLP map in Fig. 10c bears a strong resemblance to the SLP pattern in Fig. 10a and is closely related to the weakened trades throughout the subtropics. Additionally, the SST map in

Fig. 10d is dominated by the El Niño pattern in the tropical Pacific because of enhanced westerlies in the western equatorial Pacific.

Dominated by the mature stage of ENSO, strongly coupled regression maps for the MCA-III [JJASO(0) South Pacific tropical surface zonal wind and NDJFM(0) tropical Pacific SST] are shown in Figs. 10e and 10f. A strong correspondence between the zonal wind stress time series from the MCA-III and MCA-I ($r = 0.99$) indicates that the pattern in Fig. 10e is mainly caused by the previous boreal winter's South Pacific extratropical SLP anomalies.

In conclusion, the SSTAs in the central equatorial Pacific are more highly correlated with the NPMM than
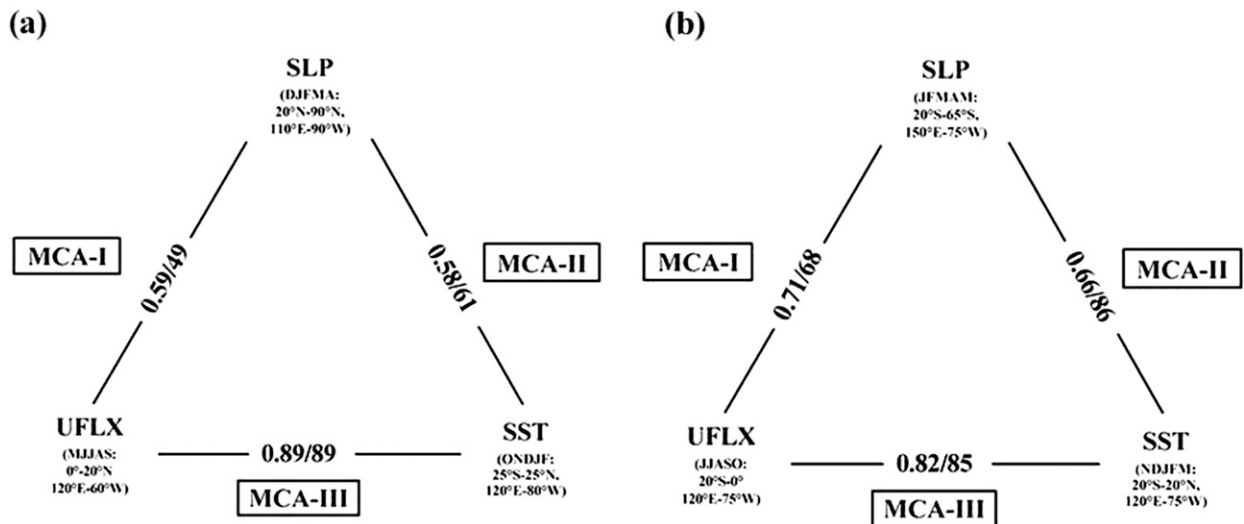
FIG. 8. Graphic illustration of the data used in the three MCAs and summary statistics from the analysis. (a),(b) Denotes results in the North Pacific and South Pacific. respectively. The summary statistics are in the following format: R/SCF, where *R* is the correlation between the associated expansion coefficient time series, and SCF is the total squared covariance fraction explained by the leading MCA mode.

the SSTAs in the eastern equatorial Pacific, whereas the SSTAs in the eastern equatorial Pacific are more highly correlated with the SPMM than the SSTAs in the central equatorial Pacific. The relationship between the South Pacific extratropical SLP variability, the zonal wind anomalies along the equator, and the tropical equatorial Pacific SSTAs are similar to the relationship between the NPO, zonal wind anomalies along the equator, and tropical equatorial Pacific SSTAs. Both relationships are illustrated in Fig. 8. During the boreal winter, the South Pacific extratropical SLP variability imparts a SST footprint (SPMM pattern) onto the ocean. The subtropical portion of the SST footprint then persists until boreal summer and extends into the tropics via WES feedback, which causes variations of the local SSTs in the eastern Pacific and forces the zonal wind anomalies along the equator, and ultimately affects ENSO formation during the following boreal autumn and winter via ocean–atmosphere coupling in the tropics.

6. Summary and discussion

The analyses presented in this paper support the hypothesis that the South Pacific extratropical variability may trigger ENSO events via the SPMM as suggested by observational data. Similar to its counterpart in the Northern Hemisphere (the NPMM), the physical processes indicate a potentially important role of South Pacific extratropical variability in predicting ENSO. Although they share nearly the same physical mechanisms, ENSO variabilities caused by the SPMM and

NPMM do have some noticeable differences: the variability of ENSO related to the NPMM is more confined to the central Pacific and has relatively less influence on the eastern equatorial Pacific, whereas the variability of ENSO related to the SPMM has less of an impact on the central equatorial Pacific. This observation is consistent with the results proposed by Zhang et al. (2014a). We also repeated the analyses using ERA Twentieth Century (ERA-20C) (Poli et al. 2013) and Extended Reconstructed SST, version 4 (ERSST.v4) (Huang et al. 2015) products, and similar results were obtained (not shown).

Compared with the NPMM, the SPMM-related SSTAs are primarily located in the eastern Pacific, particularly in the Niño-1+2 area (10°S–0°, 90°–80°W). Such differences are associated with the different spatial patterns of the NPMM and SPMM. The trade winds crossing the equator in the eastern basin favor the northward development of the SPMM via the WES feedback in both analytical studies and AGCM-slab models (e.g., Wang 2010b; Zhang et al. 2014a). Vimont et al. (2014) suggested that SST anomalies in the South Pacific may also be related to the eastern Pacific ENSO events. Zhang et al. (2014a) noted that the SPMM and NPMM appear to be related to different ENSO flavors in fully coupled models and observations, with the equatorial signature of the SPMM presenting similarities to the canonical El Niño and the equatorial signature of the NPMM presenting similarities to the central Pacific El Niño. In addition, the background winds determine the propagation of the WES feedback that is
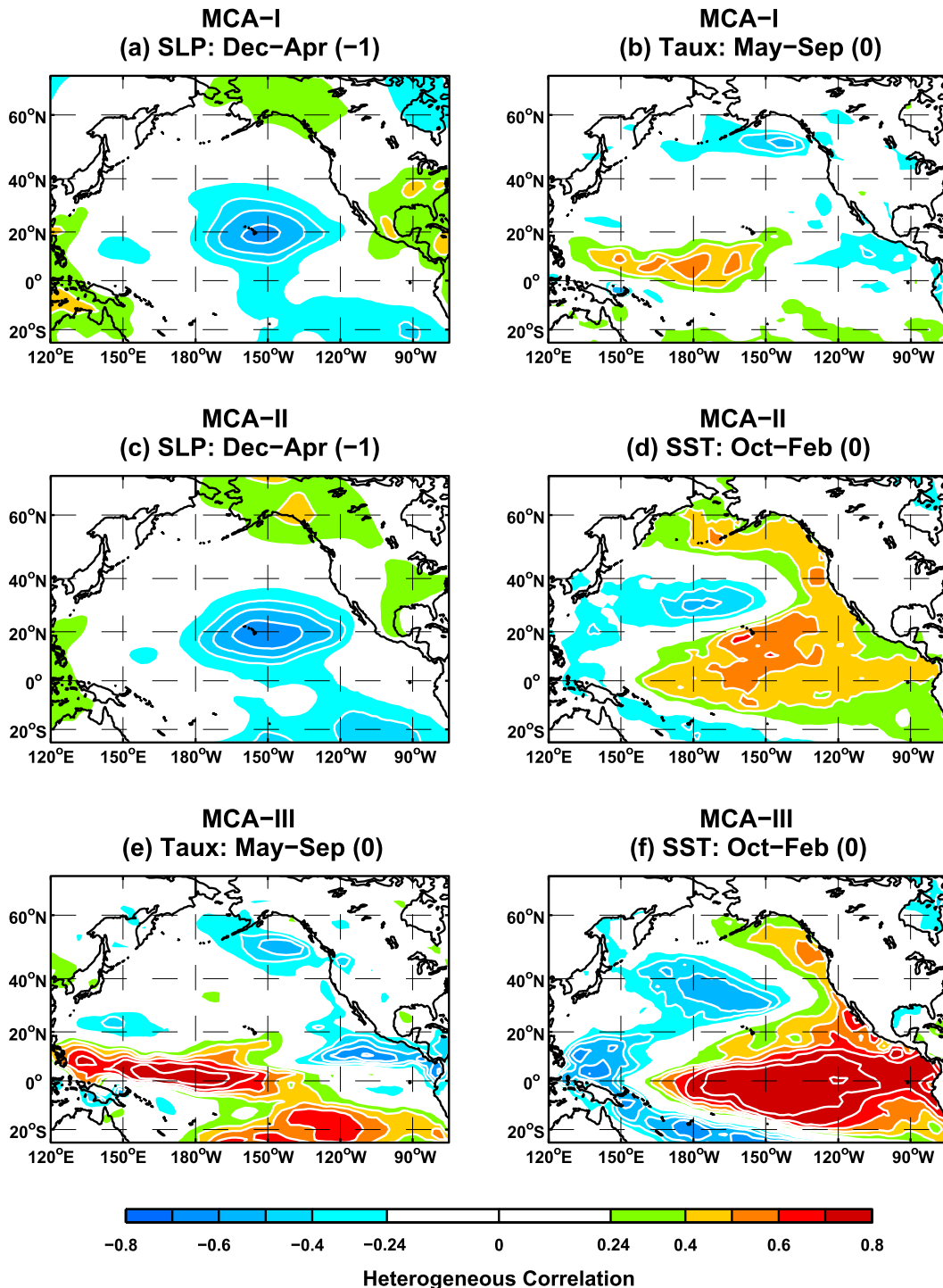
FIG. 9. Spatial properties of leading heterogeneous patterns for (top to bottom) the three separate MCA sets in the North Pacific: (a),(b) Dec–Apr(−1) SLP and May–Sep(0) surface zonal wind stress, respectively, from MCA-I; (c),(d) Dec–Apr(−1) SLP and Oct–Feb(0) SST, respectively, from MCA-II; (e),(f) May–Sep(0) surface zonal wind stress and Oct–Feb(0) SST, respectively, from MCA-III. Leading heterogeneous patterns are shown as correlation maps of the respective heterogeneous fields onto the MCA leading normalized expansion coefficients. Areas with correlations significant at the 95% confidence level are shaded.
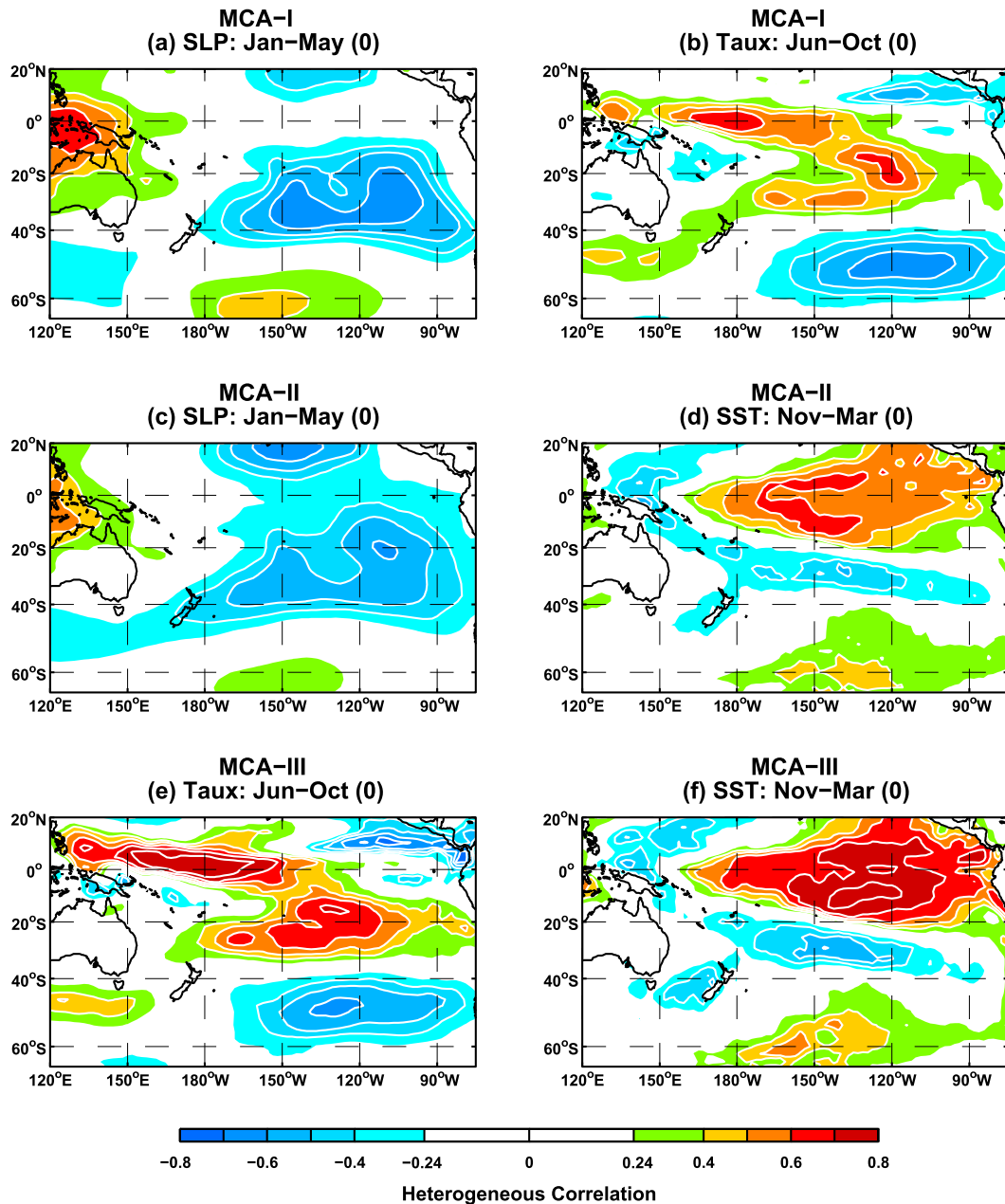
FIG. 10. As in Fig. 9, but for the South Pacific: (a),(b) Jan–May(0) SLP and Jun–Oct(0) surface zonal wind stress, respectively, from MCA-I; (c),(d) Jan–May(0) SLP and Nov–Mar(0) SST, respectively, from MCA-II; (e),(f) Jun–Oct(0) surface zonal wind stress and Nov–Mar(0) SST, respectively, from MCA-III.

fundamental for both PMMs (Zhang et al. 2014b). The analyses provided in the present paper reaffirm these hypotheses. In addition to the WES feedback, the Pacific cold-tongue-related ocean dynamics may also contribute to the northward extension of the SPMM in fully coupled models and observations (Mitchell and Wallace 1992; Liu and Xie 1994). Because of its nonlinearity, ENSO cannot be perfectly or absolutely removed from observations. Thus, further research is required to

address the relationship between ENSO and NPMM–SPMM.

To check the robustness of the PMMs' seasonality, the NPMM–SPMM were also calculated for the post-satellite era using 10-m wind data from ERA-Interim reanalysis (Dee et al. 2011) and SSTs from NOAA optimum interpolation SST, version 2 (OISSTv2) (Reynolds et al. 2002). In this calculation, the SST seasonality of the NPMM peaks in March–May and the SST

seasonality of the SPMM peaks in January–March. Other spatial and temporal characteristics are similar to that in Fig. 3 (not shown), which indicates that the temporal features of the NPMM–SPMM differ between the different datasets, especially for the SPMM. But these differences do not affect the physical nature of the relationship between ENSO and PMMs.

The definition of SPMM remains controversial. The SPMM and the observed subtropical dipole mode (e.g., Wang 2010a) in the South Pacific share similar spatial patterns that exhibit a northeast–southwest-tilted SST dipole pattern. Zhang et al. (2014a) noted that it is possible that the subtropical dipole mode represents a snapshot of the propagation of the SPMM on the seasonal time scale, and a comprehensive comparison of both modes is needed. Ding et al. (2015) claimed that the quadrupole SST variability in the extratropical South Pacific triggered by the midlatitude South Pacific atmospheric variability may have an additional influence on ENSO, whereas it appears that the SPMM is simply a component of the quadrupole SST pattern near the equator in their study. Their study also demonstrated that South Pacific extratropical forcing is relatively independent of North Pacific extratropical forcing, and they showed that the NPO and Pacific–South American (PSA) appear to have different relationships with different types of El Niño. However, although the South Pacific extratropical SLP pattern in Fig. 10a bears a strong resemblance to the PSA pattern shown in Fig. 1 of Mo (2000), the correlation between the first (second) [PSA1 (PSA2)] principal component of the empirical orthogonal function of the 500-mb mean height anomalies in the South Pacific and the SPMM 10-m wind expansion coefficient is not significant (not shown), which indicates that the SPMM may not be related to the PSA pattern.

Recent reports have indicated that ENSO events are strongly influenced by the NPMM or SPMM in reality. In the boreal summer/autumn of 2012, the SST cooling in the subtropical North Pacific, which was caused by the negative phase of the NPMM, induced strong easterly and low-level divergence anomalies that suppressed the development of westerly and convection anomalies over the central equatorial Pacific. The surface warming over the equatorial Pacific was decoupled from the surface wind forcing and subsurface thermocline variability, thereby inhibiting its further development into a mature El Niño in the boreal autumn/winter of 2012/13 (Su et al. 2014). In the boreal summer of 2014, a suppressed ocean–atmosphere interaction, caused by anomalous easterly winds in the eastern equatorial Pacific, hindered the development of El Niño. These winds were related to negative SSTAs in the southeastern subtropical Pacific, which are associated with the variability of the

SPMM (Min et al. 2015). Moreover, the negative phase of the interdecadal Pacific oscillation (IPO) laid the foundation for the persistence of cooler SSTAs and enhanced trade winds in the southeastern subtropical Pacific after the year 2000, which implies that the phase of the IPO may also influence the phase of the SPMM and further influence the development of ENSO.

This study has several potential implications. First, the different influences of the NPMM and SPMM on ENSO, which are associated with the North and South Pacific extratropical variability, were compared in both hemispheres. The differences may account for different ENSO flavors, which are particularly important for the prediction of ENSO. Second, the NPMM and SPMM may also inhibit the development of ENSO events under special backgrounds, which is similar to the 2012 and 2014 ENSO events. This study is supported by both observed events (e.g., Su et al. 2014; Min et al. 2015) and model results (e.g., Zhang et al. 2014a), thus supporting our results and interpretations. Furthermore, when considering the origins of the SPMM, other questions remain. Although the SPMM originates from the South Pacific extratropics independent of ENSO in the previous boreal winter (Fig. 4b), the question of whether the SPMM originates solely or partly from the remote tropical forcing in other seasons according to fully coupled models and observation data requires further study.

This study emphasizes the importance of climatic variability of both the Northern and Southern Hemispheres in the tropical Pacific climate, and it suggests that both the NPMM and SPMM in the subtropical Pacific can be important ENSO predictors in the future. Therefore, forecasts of a particular ENSO flavor may be improved, although such forecasts will certainly require further research.

REFERENCES

Ashok, K., S. K. Behera, S. A. Rao, H. Weng, and T. Yamagata, 2007: El Niño Modoki and its possible teleconnection. *J. Geophys. Res.*, **112**, C11007, doi:10.1029/2006JC003798.

Barnston, A. G., M. K. Tippett, M. L. L'Heureux, S. Li, and D. G. DeWitt, 2012: Skill of real-time seasonal ENSO model predictions during 2002–11: Is our capability increasing? *Bull. Amer. Meteor. Soc.*, **93**, 631–651, doi:10.1175/BAMS-D-11-00111.1.

Bretherton, C. S., C. Smith, and J. M. Wallace, 1992: An intercomparison of methods for finding coupled patterns in climate data. *J. Climate*, **5**, 541–560, doi:10.1175/1520-0442(1992)005<0541: AIOMFF>2.0.CO;2.

Chang, P., L. Ji, and H. Li, 1997: A decadal climate variation in the tropical Atlantic Ocean from thermodynamic air–sea interactions. *Nature*, **385**, 516–518, doi:10.1038/385516a0.

——, L. Zhang, R. Saravanan, D. J. Vimont, J. C. H. Chiang, L. Ji, H. Seidel, and M. K. Tippett, 2007: Pacific meridional mode and El Niño–Southern Oscillation. *Geophys. Res. Lett.*, **34**, L16608, doi:10.1029/2007GL030302.

Chen, D., and Coauthors, 2015: Strong influence of westerly wind bursts on El Niño diversity. *Nat. Geosci.*, **8**, 339–345, doi:10.1038/ngeo2399.

Chiang, J. C. H., and D. J. Vimont, 2004: Analogous Pacific and Atlantic meridional modes of tropical atmosphere–ocean variability. *J. Climate*, **17**, 4143–4158, doi:10.1175/JCLI4953.1.

Dee, D., and Coauthors, 2011: The ERA-Interim reanalysis: Configuration and performance of the data assimilation system. *Quart. J. Roy. Meteor. Soc.*, **137**, 553–597, doi:10.1002/qj.828.

Deser, C., and J. M. Wallace, 1990: Large-scale atmospheric circulation features of warm and cold episodes in the tropical Pacific. *J. Climate*, **3**, 1254–1281, doi:10.1175/1520-0442(1990)003<1254: LSACFO>2.0.CO;2.

Di Lorenzo, E., G. Liguori, N. Schneider, J. C. Furtado, B. T. Anderson, and M. A. Alexander, 2015: ENSO and meridional modes: A null hypothesis for Pacific climate variability. *Geophys. Res. Lett.*, **42**, 9440–9448, doi:10.1002/2015GL066281.

Ding, R.-Q., J.-P. Li, and Y.-H. Tseng, 2015: The impact of South Pacific extratropical forcing on ENSO and comparisons with the North Pacific. *Climate Dyn.*, **44**, 2017–2034, doi:10.1007/s00382-014-2303-5.

Guilyardi, E., A. Wittenberg, A. Fedorov, M. Collins, C. Wang, A. Capotondi, G. J. van Oldenborgh, and T. Stockdale, 2009: Understanding El Niño in ocean–atmosphere general circulation models: Progress and challenges. *Bull. Amer. Meteor. Soc.*, **90**, 325–340, doi:10.1175/2008BAMS2387.1.

Huang, B., and Coauthors, 2015: Extended Reconstructed Sea Surface Temperature version 4 (ERSST.v4). Part I: Upgrades and intercomparison. *J. Climate*, **28**, 911–930, doi:10.1175/JCLI-D-14-00006.1.

Kalnay, and Coauthors, 1996: The NCEP/NCAR 40-Year Reanalysis Project. *Bull. Amer. Meteor. Soc.*, **77**, 437–470, doi:10.1175/1520-0477(1996)077<0437:TNYRP>2.0.CO;2.

Kao, H.-Y., and J.-Y. Yu, 2009: Contrasting eastern Pacific and central Pacific types of El Niño. *J. Climate*, **22**, 615–632, doi:10.1175/2008JCLI2309.1.

Kug, J. S., F. F. Jin, and S. I. An, 2009: Two types of El Niño events: Cold tongue El Niño and warm pool El Niño. *J. Climate*, **22**, 1499–1515, doi:10.1175/2008JCLI2624.1.

Kushnir, Y., R. Seager, J. Miller, and J. C. H. Chiang, 2002: A simple coupled model of tropical Atlantic decadal climate variability. *Geophys. Res. Lett.*, **29**, 2133, doi:10.1029/2002GL015874.

Liu, Z., and S.-P. Xie, 1994: Equatorward propagation of coupled air–sea disturbances with application to the annual cycle of the eastern tropical Pacific. *J. Atmos. Sci.*, **51**, 3807–3822, doi:10.1175/1520-0469(1994)051<3807: EPOCAD>2.0.CO;2.

McPhaden, M. J., and Coauthors, 1998: The Tropical Ocean-Global Atmosphere observing system: A decade of progress. *J. Geophys. Res.*, **103**, 14 169–14 240, doi:10.1029/97JC02906.

Min, Q.-Y., J.-Z. Su, R.-H. Zhang, and X.-Y. Rong, 2015: What hindered the El Niño pattern in 2014? *Geophys. Res. Lett.*, **42**, 6762–6770, doi:10.1002/2015GL064899.

Mitchell, T. P., and J. M. Wallace, 1992: On the annual cycle in equatorial convection and sea surface temperature. *J. Climate*, **5**, 1140–1156, doi:10.1175/1520-0442(1992)005<1140:TACIEC>2.0.CO;2.

Mo, K. C., 2000: Relationships between low-frequency variability in the Southern Hemisphere and sea surface temperature anomalies. *J. Climate*, **13**, 3599–3610, doi:10.1175/1520-0442(2000)013<3599: RBLFVI>2.0.CO;2.

Nobre, P., and J. Shukla, 1996: Variations of sea surface temperature, wind stress, and rainfall over the tropical Atlantic and South America. *J. Climate*, **9**, 2464–2479, doi:10.1175/1520-0442(1996)009<2464:VOSSTW>2.0.CO;2.

Pierce, D. W., T. P. Barnett, and M. Latif, 2000: Connections between the Pacific Ocean tropics and midlatitudes on decadal timescales. *J. Climate*, **13**, 1173–1194, doi:10.1175/1520-0442(2000)013<1173: CBTPOT>2.0.CO;2.

Poli, P., and Coauthors, 2013: The data assimilation system and initial performance evaluation of the ECMWF pilot reanalysis of the 20th-century assimilating surface observations only (ERA-20C). ERA Rep. Series, Rep. 14, 59 pp. [Available online at http://www.ecmwf.int/en/elibrary/11699-data-assimilation-system-and-initial-performance-evaluation-ecmwf-pilot-reanalysis.]

Reynolds, R. W., N. A. Rayner, T. M. Smith, D. C. Stokes, and W. Wang, 2002: An improved in situ and satellite SST analysis for climate. *J. Climate*, **15**, 1609–1625, doi:10.1175/1520-0442(2002)015<1609:AIISAS>2.0.CO;2.

Rogers, J. C., 1981: The North Pacific Oscillation. *J. Climatol.*, **1**, 39–57, doi:10.1002/joc.3370010106.

Servain, J., I. Wainer, J. P. McCreary, and A. Dessier, 1999: Relationship between the equatorial and meridional modes of climatic variability in the tropical Atlantic. *Geophys. Res. Lett.*, **26**, 485–488, doi:10.1029/1999GL900014.

Su, J.-Z., B.-Q. Xiang, B. Wang, and T. Li, 2014: Abrupt termination of the 2012 Pacific warming and its implication on ENSO prediction. *Geophys. Res. Lett.*, **41**, 9058–9064, doi:10.1002/2014GL062380.

U.S. CLIVAR ENSO Diversity Working Group, 2013: Report on the ENSO Diversity Workshop. U.S. CLIVAR Rep. 2011-1, U.S. CLIVAR Project Office, 20 pp. [Available online at http://www.usclivar.org/sites/default/files/meetings/ENSO_Diversity_Workshop_Report.pdf.]

Vimont, D. J., D. S. Battisti, and A. C. Hirst, 2001: Footprinting: A seasonal connection between the tropics and mid-latitudes. *Geophys. Res. Lett.*, **28**, 3923–3926, doi:10.1029/2001GL013435.

——, ——, and ——, 2003a: The seasonal footprinting mechanism in the CSIRO general circulation models. *J. Climate*, **16**, 2653–2667, doi:10.1175/1520-0442(2003)016<2653:TSFMIT>2.0.CO;2.

——, J. M. Wallace, and D. S. Battisti, 2003b: The seasonal footprinting mechanism in the Pacific: Implications for ENSO. *J. Climate*, **16**, 2668–2675, doi:10.1175/1520-0442(2003)016<2668: TSFMIT>2.0.CO;2.

——, M. Alexander, and A. Fontaine, 2009: Midlatitude excitation of tropical variability in the Pacific: The role of thermodynamic coupling and seasonality. *J. Climate*, **22**, 518–534, doi:10.1175/2008JCLI2220.1.

——, M. A. Alexander, and M. Newman, 2014: Optimal growth of Central and East Pacific ENSO events. *Geophys. Res. Lett.*, **41**, 4027–4034, doi:10.1002/2014GL059997.

Wang, F., 2010a: Subtropical dipole mode in the Southern Hemisphere: A global view. *Geophys. Res. Lett.*, **37**, L10702, doi:10.1029/2010GL042750.

——, 2010b: Thermodynamical coupled modes in the tropical atmosphere–ocean: An analytical solution. *J. Atmos. Sci.*, **67**, 1667–1677, doi:10.1175/2009JAS3262.1.

Xie, S.-P., and S. G. H. Philander, 1994: A coupled ocean–atmosphere model of relevance to the ITCZ in the eastern Pacific. *Tellus*, **46A**, 340–350, doi:10.1034/j.1600-0870.1994.t01-1-00001.x.

Yu, J.-Y., H.-Y. Kao, and T. Lee, 2010: Subtropics-related interannual sea surface temperature variability in the equatorial central Pacific. *J. Climate*, **23**, 2869–2884, doi:10.1175/2010JCLI3171.1.

Zhang, H., A. Clement, and P. Di Nezio, 2014a: The South Pacific meridional mode: A mechanism for ENSO-like variability. *J. Climate*, **27**, 769–783, doi:10.1175/JCLI-D-13-00082.1.

——, C. Deser, A. Clement, and R. Tomas, 2014b: Equatorial signatures of the Pacific Meridional Modes: Dependence on mean climate state. *Geophys. Res. Lett.*, **41**, 568–574, doi:10.1002/2013GL058842.

Zhang, R., and G. Zhao, 2001: Meridional wind stress anomalies over the tropical Pacific and the onset of El Niño. Part II: Dynamical analysis. *Adv. Atmos. Sci.*, **18**, 1053–1065, doi:10.1007/s00376-001-0022-4.

——, ——, and Y. Tan, 2001: Meridional wind stress anomalies over the tropical Pacific and the onset of El Niño. Part I: Data analysis. *Adv. Atmos. Sci.*, **18**, 467–480, doi:10.1007/s00376-001-0038-9.